Chapter 4

Serial setup

An interferometric approach to shaping of the phase, the amplitude, and the polarization shaping has its challenges. One of them is the necessity of exact overlap of two orthogonally polarized laser beams, the other is the issue of the relative phase stability. The resulting polarization of the pulses is in this case very sensitive to mechanical vibrations of the setup. In this Chapter, a different method is proposed and experimentally realized which does not demand interferometric stability. A double layer modulator is either capable of phase and amplitude or phase and polarization manipulation. To realize simultaneous and independent control over the phase, amplitude, and polarization a new shaper setup is introduced. It takes advantage of laser pulses passing through a spatial light modulator (SLM) twice and therefore effectively utilizing a four liquid crystal mask configuration.

First, the Jones vector formalism is used to analyze a construction consisting of the layers with $\pm 45°$ optical axes including the four array solution based on two double layer modulators arranged sequentially. Next, the experimental setup is demonstrated and then it is followed by equalizing of the grating polarization sensitive transmission. After the capabilities of the setup are tested, trial pulses are generated and measured.

4.1 Mathematical description

The natural choice, in order to expand capabilities of a modulator, is to add an extra crystal layer to the double "crystal sandwich", which leaves us with

two choices of configuration for such a three layer modulator. It is necessary to use a polarizer to achieve amplitude modulation, but placed after the last array it will eliminate the option of polarization tailoring. Thus, it could be placed either after the first (a) or second layer (b). Let us define at this point, for simplicity of the calculations, matrices for rotated nematic crystals.

$$M_{\beta}[\phi_x] = R[\beta] \cdot LC[\phi_x] \cdot R[-\beta]$$

When the polarizer is placed after the first array then the matrix

$$\begin{aligned} M_{45^\circ,PP,45^\circ,-45^\circ} &= M_{45^\circ}[\phi_c] \cdot M_{-45^\circ}[\phi_b] \cdot PP \cdot M_{45^\circ}[\phi_a] = \\ e^{\frac{1}{2}i(\phi_a+\phi_b+\phi_c)} &\begin{bmatrix} \cos[\frac{\phi_a}{2}]\cos[\frac{\phi_b-\phi_c}{2}] & i\sin[\frac{\phi_a}{2}]\cos[\frac{\phi_b-\phi_c}{2}] \\ -i\cos[\frac{\phi_a}{2}]\sin[\frac{\phi_b-\phi_c}{2}] & \sin[\frac{\phi_a}{2}]\sin[\frac{\phi_b-\phi_c}{2}] \end{bmatrix} \end{aligned} \tag{4.1}$$

is returned, where PP denotes a P aligned polarizer. Afterwards the electric field is calculated.

$$\begin{aligned} \overrightarrow{E}_{45^\circ,PP,45^\circ,-45^\circ} &= M_{45^\circ,P,45^\circ,-45^\circ} \cdot E_0 e^{i\omega t} \begin{bmatrix} 1 \\ 0 \end{bmatrix} = \\ E_0 e^{i\omega t} e^{\frac{1}{2}i(\phi_a+\phi_b+\phi_c)} &\cos[\frac{\phi_a}{2}] \begin{bmatrix} \cos[\frac{\phi_b-\phi_c}{2}] \\ -i\sin[\frac{\phi_b-\phi_c}{2}] \end{bmatrix} \end{aligned} \tag{4.2}$$

When the phase (φ),transmission (T), and polarization vector ($\widetilde{p}$) are extracted from Eq. 4.2, it is apparent that independent handling of these components is achievable.

$$\begin{aligned} \varphi_{45^\circ,PP,45^\circ,-45^\circ} &= \frac{1}{2}(\phi_a + \phi_b + \phi_c) \\ T_{45^\circ,PP,45^\circ,-45^\circ} &= \cos^2[\frac{\phi_a}{2}] \\ \widetilde{p}_{45^\circ,PP,45^\circ,-45^\circ} &= \begin{bmatrix} \cos[\frac{\phi_b-\phi_c}{2}] \\ -i\sin[\frac{(\phi_b-\phi_c)}{2}] \end{bmatrix} \end{aligned} \tag{4.3}$$

The same procedure can be repeated for the polarizer placed in between the second (b) and third layer (c) of nematic crystals. This combination of crystals and polarizer gives matrix 4.4.

$$M_{45^\circ,-45^\circ,PP,45^\circ} = M_{45^\circ}[\phi_c] \cdot PP \cdot M_{-45^\circ}[\phi_b] \cdot M_{45^\circ}[\phi_a] =$$

$$e^{\frac{1}{2}i(\phi_a+\phi_b+\phi_c)}\begin{bmatrix}\cos[\frac{\phi_a-\phi_b}{2}]\cos[\frac{\phi_c}{2}] & i\sin[\frac{\phi_a-\phi_b}{2}]\cos[\frac{\phi_c}{2}]\\ i\cos[\frac{\phi_a-\phi_b}{2}]\sin[\frac{\phi_c}{2}] & -\sin[\frac{\phi_a-\phi_b}{2}]\sin[\frac{\phi_c}{2}]\end{bmatrix} \tag{4.4}$$

The outgoing electric field is described by

$$\overrightarrow{E}_{45^\circ,-45^\circ,PP,45^\circ} = E_0 e^{i\omega t} e^{\frac{1}{2}i(\phi_a+\phi_b+\phi_c)}\cos[\frac{\phi_a-\phi_b}{2}]\begin{bmatrix}\cos[\frac{\phi_c}{2}]\\ i\sin[\frac{(\phi_c)}{2}]\end{bmatrix}. \tag{4.5}$$

Hence phase, transmission, and polarization are expressed as follows.

$$\begin{aligned}\varphi_{45^\circ,-45^\circ,PP,45^\circ} &= \frac{1}{2}(\phi_a+\phi_b+\phi_c)\\ T_{45^\circ,-45^\circ,PP,45^\circ} &= \cos^2[\frac{\phi_a-\phi_b}{2}]\\ \widetilde{p}_{45^\circ,-45^\circ,PP,45^\circ} &= \begin{bmatrix}\cos[\frac{\phi_c}{2}]\\ i\sin[\frac{(\phi_c)}{2}]\end{bmatrix}\end{aligned} \tag{4.6}$$

Both types of arrangements offer independent access to the phase, amplitude and limited control to the polarization of an electric field and there is basically no distinction from mathematical and practical point of view which solution is better to be carried out.

The above calculations and considerations are purely theoretical, since, according to the authors knowledge, such setups have not been implemented yet. Since three layer modulators are not purchasable yet, it is pragmatic to consider using two double layer modulators with a polarizer between them. These devices are now available and most important, come generally with removable polarizers before and after the crystal arrays. The Jones matrix of this configuration is calculated in 4.7

$$\begin{aligned}M_{serial} = M_{-45^\circ}[\phi_d]\cdot M_{45^\circ}[\phi_c]\cdot PP\cdot M_{-45^\circ}[\phi_b]\cdot M_{45^\circ}[\phi_a] =\\ e^{\frac{1}{2}i(\phi_a+\phi_b+\phi_c+\phi_d)}\begin{bmatrix}\cos[\frac{\phi_a-\phi_b}{2}]\cos[\frac{\phi_c-\phi_d}{2}] & i\sin[\frac{\phi_a-\phi_b}{2}]\cos[\frac{\phi_c-\phi_d}{2}]\\ i\cos[\frac{\phi_a-\phi_b}{2}]\sin[\frac{\phi_c-\phi_d}{2}] & -\sin[\frac{\phi_a-\phi_b}{2}]\sin[\frac{\phi_c-\phi_d}{2}]\end{bmatrix}\end{aligned} \tag{4.7}$$

from which the electric field is obtained

$$\overrightarrow{E}_{serial} = E_0 e^{i\omega t} e^{-\frac{1}{2}i(\phi_a+\phi_b+\phi_c+\phi_d)}\cos[\frac{\phi_a-\phi_b}{2}]\begin{bmatrix}\cos[\frac{\phi_c-\phi_d}{2}]\\ i\sin[\frac{\phi_c-\phi_d}{2}]\end{bmatrix}. \tag{4.8}$$

Phase, transmission, and polarization are given by 4.9.

$$\varphi_{serial} = \frac{1}{2}(\phi_a + \phi_b + \phi_c + \phi_d)$$
$$T_{serial} = \cos^2[\frac{\phi_a - \phi_b}{2}]$$
$$\widetilde{p}_{serial} = \begin{bmatrix} \cos[\frac{\phi_c - \phi_d}{2}] \\ i\sin[\frac{(\phi_c - \phi_d)}{2}] \end{bmatrix} \tag{4.9}$$

Adding an extra crystal layer does not improve the setup comparing to the three layers configurations and unfortunately it has exactly the same limitation for manipulating the polarization, as the two or three layer configuration, described above. It is simply another way to obtain a tree layer configuration by combining double layer modulators.

4.2 Experimental setup

Building a shaper containing four nematic crystal arrays would require two double array modulators placed in a fourier plane. Instead, one can transmit the spectral components of a fs pulse twice through different regions of a double array modulator, which is a less expensive solution [77]. The layout of this construction is presented in Figure 4.1.

The optical layout itself is similar to the single pass shaper built for the SLM-640 from CRi. The different arrangement of the gratings allows the spectral components to pass right from the center of the modulator, when looking from the direction of the incoming beam. Then, the beam is propagated through a P orientated polarizer and reflected back on the second grating. It hits the grating at exactly the same point, but the angle is chosen for the spectrum to pass left from the optical axis. This way, on the second round different pixels of the modulator are illuminated. Effectively, this confinement is a four array modulator with a polarizer in between the second and third array. The natural disadvantage of this solution is a half resolution comparing to the single pass shaper, as the spectrum is influenced by a half of the pixels.

The subject of resolution is is followed by an issue of the necessary pixel assignment from the first pass to the second. In the general case, when

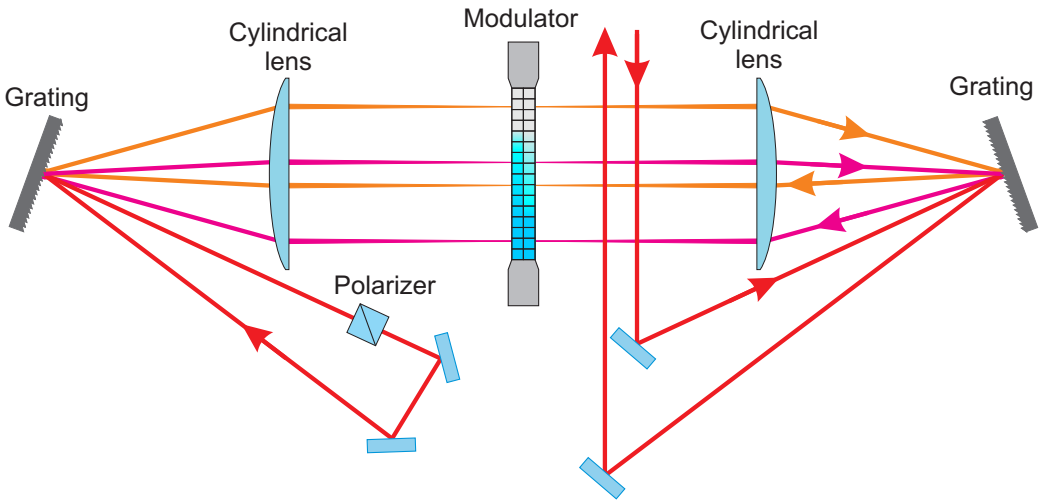

Figure 4.1: The serial shaper configuration. The laser beam enters the first grating of density 600 $lines/mm$, as the arrow (right top part of the figure) indicates, and its spectral components are being spatially separated and collimated by the cylindrical lens with a focal length of $250mm$. Then they are transmitted through a modulator placed in the Fourier plane and hit the second grating. Afterwards the beam is send through the polarizer and is redirected again on the second grating at a different incident angle. The spectral components are sent a second time through another part of the modulator, enter the first grating and leave the setup.

using different incidence angles on the grating, the dispersion of the spectrum will differ as well, and it will affect the spatial distribution of the spectrum. Although for a small change of the angle, this effect should not be significant. A simulation of the grating dispersion has been made to estimate the order of this difference. The spectrum of a determined bandwidth was propagated for two different incidence angles and then the spatial wavelength spread was calculated. By comparing these spatial spreads for the same spectrum one can estimate the errors by the theoretical overlap of the pixels. The results of this simulation for a grating density of 600 lines/mm, a distance from the grating 250 mm, a grating angle of 5°, and incidence angles of 15° and 20° are presented in Figure 4.2.

It is hard to distinguish any differences between the spatial distributions of the spectrum for the two passes presented in the upper plot in Figure 4.2, apart from the obvious shift in space. If the spread would be identical, then

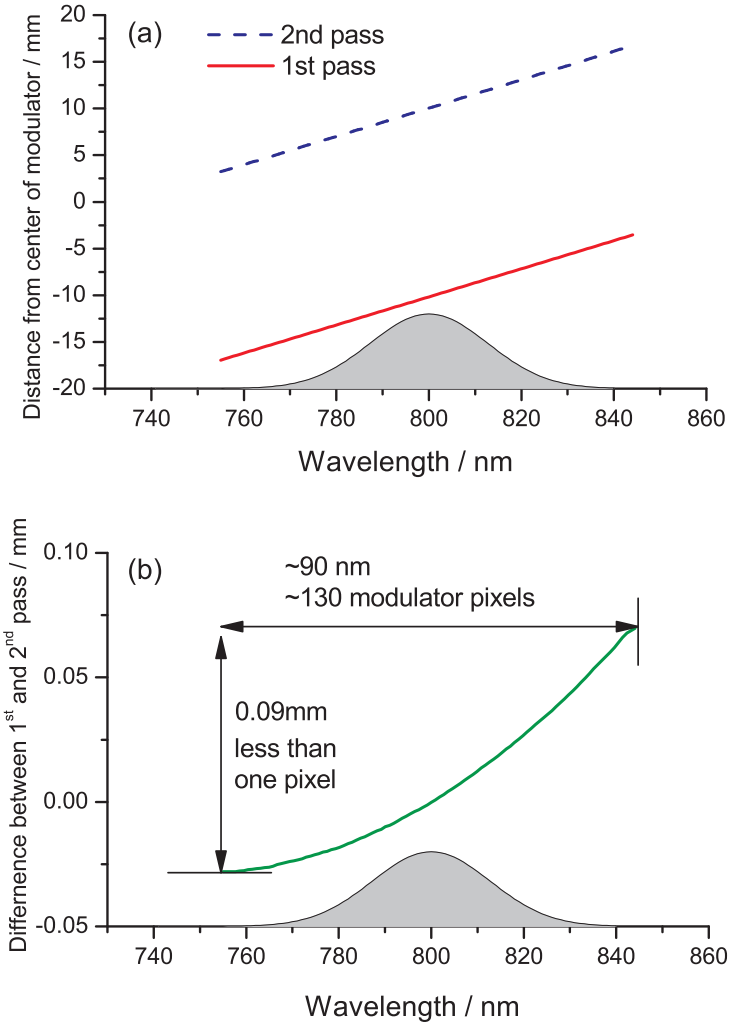

Figure 4.2: Graph (a) shows the wavelength distribution on the modulator in the first and the second pass of the serial shaper setup. Graph (b) presents the difference of the wavelength distribution for the first and the second pass with the extracted difference for the central wavelength, so the curve passes zero at $\lambda = 800$ nm. The used laser spectrum is indicated on both graphs by a gray Gaussian function.

the difference of the spatial spectrum distribution should be a flat function $f(\lambda) = const$. This difference is plotted below on Figure 4.2. On the bandwidth of 90 nm the change is 90 μm. Translating this to the pixel picture, it corresponds to the situation of illuminating 130 pixels in the first pass and 131 in the second. The assumed bandwidth of 90 nm is in fact a spectrum with 30 nm FWHM, which means that on the side wings of this spectrum the intensity is very low. Additionally, the dispersion errors are probably smaller then chromatic abberations of the used BK7 lenses of a focal length of 250 mm. Concluding, for a given grating and angles the calculated mismatch of the pixel pairs suggest that it can be neglected in the setup, which is well supported by the experimental results.

4.3 The polarization manipulation

According to Expression 4.9 the polarization of the fs pulse spectral components can be controlled by a difference of the phase shifts $(\phi_c - \phi_d)$ in the second pass. To confirm this relation experimentally, scans of phase shift difference versus power transmitted through a polarizer were made. As one could predict from the theoretical electric field description 4.8, the curves can be very well approximated by $A\cos^2[\frac{\phi_c-\phi_d}{2}]$ for the P and $A\sin^2[\frac{\phi_c-\phi_d}{2}]$ for the S orientated polarizer, where A is the amplitude. Thus, the results of this scan proves the polarization manipulation. Unfortunately, but not unexpectedly, the amplitudes of these curves differ for the P and S orientated polarizer.

In the serial setup the light is being transmitted four times through gratings and some intensity is lost in comparison with "single pass" shaper due to the efficiency of the used gratings. Moreover, when manipulation of polarization occurs in the second pass, then the transmission of the serial shaper becomes polarization dependent, while the grating efficiency is polarization sensitive. Fortunately, only the last reflection is responsible for this effect. To examine the independence of polarization manipulation from the amplitude, the same scans of phase shift difference $(\phi_c - \phi_d)$ ware performed, but this time without polarizer. Scans with and without polarizer are presented in Figure 4.3.

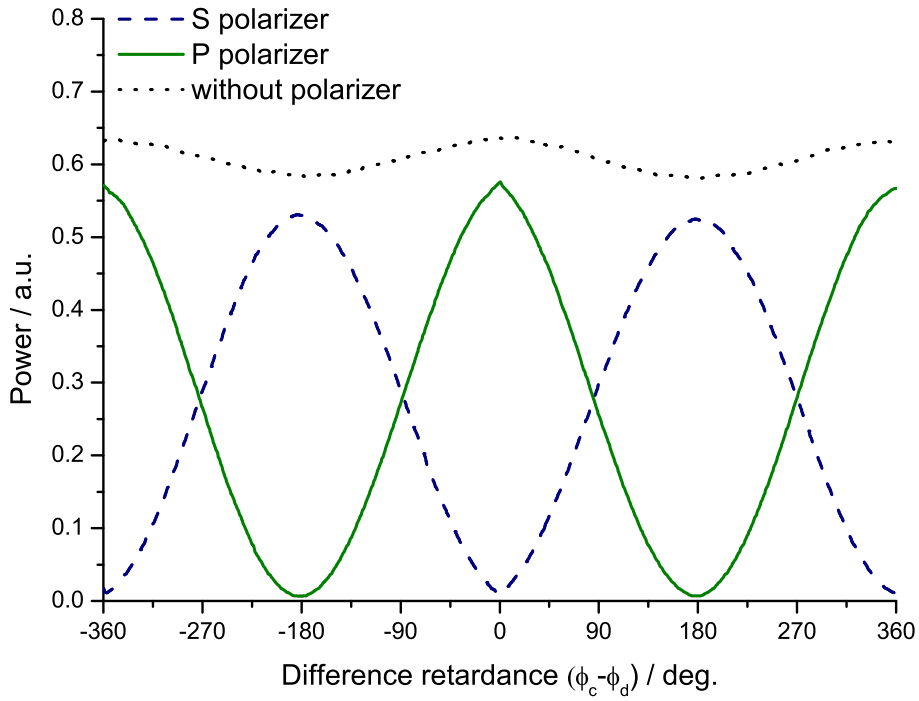

Figure 4.3: Scan of the difference retardance ($\phi_c - \phi_d$) of a LC array versus the transmitted intensity through the serial shaper and a polarizer. The measurement was performed for P and S orientated polarizers and as well without, as indicated in the Figure. The effect of polarization manipulation is visible on the curves with polarizer and the polarization sensitive transmission of the grating on the scan without the polarizer.

The modulation introduced by the reflection efficiency of the used diffraction grating of 600 lines/mm is about 10% from P to S. This relatively low change in efficiency for the grating needs to be taken into account when generating polarization shaped fs pulses. One possible way to balance the polarization dependent transmission is to use Brewster plates. Placed in the laser beam after the shaper, they can be orientated in a way that the P component gets reduced in intensity much more than the S component. By careful alignment it is possible to equalize the intensity of both components [78]. That way, the intensity of the P polarization gets reduced much more than for S

direction and so the overall transmission is finally the same. Regrettably, for larger bandwidths the Brewster angle varies across the spectrum which in consequence will lead a wavelength dependent intensity attenuation for both polarization components. Alternatively, one can counteract the grating effect using the amplitude filtering even before the polarization shaping occurs. A polarization coupled transmission filter attenuates the intensity of all polarization states to the level of pure S polarization. Equalizing of the components intensities is achieved by software, thus the method does not involve any additional optical elements in the beam, and also the procedure of finding the correct settings can be easily automated when changing gratings or wavelengths.

To properly design such a filter let us examine the grating effect in the Jones matrices description. To simplify our considerations let us focus only on the reflectivity of the diffraction grating and omit the dispersion. In this manner one can treat a grating like some inefficient polarizer that does transmit as well the "wrong" polarization. Thus, the grating matrix would take the form

$$G = \begin{pmatrix} 1 & 0 \\ 0 & g \end{pmatrix} . \tag{4.10}$$

The transmission of this element is set to 1 for P and g^2 for S polarized light. The g^2 can be regarded as the relative efficiency of the grating for the S component in comparison to the efficiency of the P component. Further simplifications can be made here regarding the modulator. Namely, one layer is enough to manipulate the polarization when excluding other parameters.

$$G \cdot M_{45^\circ}[\phi] \cdot P = \begin{bmatrix} \cos[\frac{\phi}{2}] \\ ig \sin[\frac{\phi}{2}] \end{bmatrix} \tag{4.11}$$

Hence the measured value in the experiment is the intensity one has to square the electric field amplitudes for both components and add them. This operation has been done for the shaper without the polarizer in the outgoing beam and with one, P and S orientated. The results are shown in 4.12.

$$I_{grat} = I_0(\cos^2[\frac{\phi}{2}] + g^2 \sin^2[\frac{\phi}{2}])$$

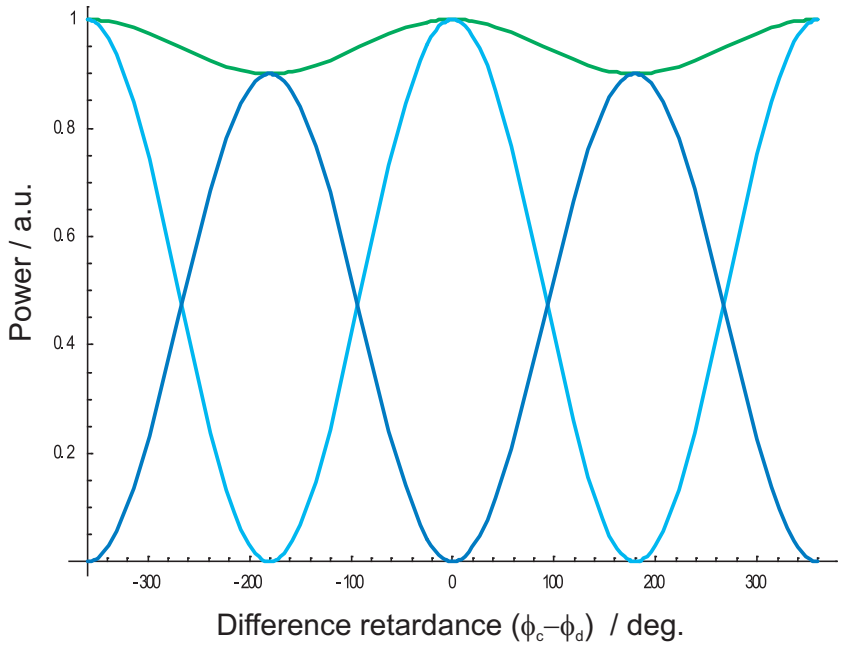

Figure 4.4: Simulation of the difference retardance scan versus intensity of the outgoing beam for a grating with the g^2 parameter equal to 0.9. Three curves represent scans done with P and S orientated polarizer and without one in a beam. The amplitude of the scan for an S orientated polarizer is significantly smaller than in the example of a P orientated polarizer, the scan without polarizer shows a modulation, which is a good qualitative agreement with the experiment.

$$I_{grat,Ppol} = I_0 \cos^2[\frac{\phi}{2}]$$
$$I_{grat,Spol} = I_0 g^2 \sin^2[\frac{\phi}{2}] \tag{4.12}$$

The simulated intensities which are displayed in Figure 4.4 resemble the measured curves from Figure 4.3 very well. The proper amplitude filter should result in a constant intensity after the shaper while scanning the retardance responsible for the polarization manipulation. Therefore the introduced amplitude filter function has to be coupled with the retardance. Consequently, the filter function is the reciprocal of the calculated intensity function I_{grat} from equation 4.12 with a normalization factor g^2. Applying this filter for the amplitude requires taking a square root of it, since $I \sim E^2$.

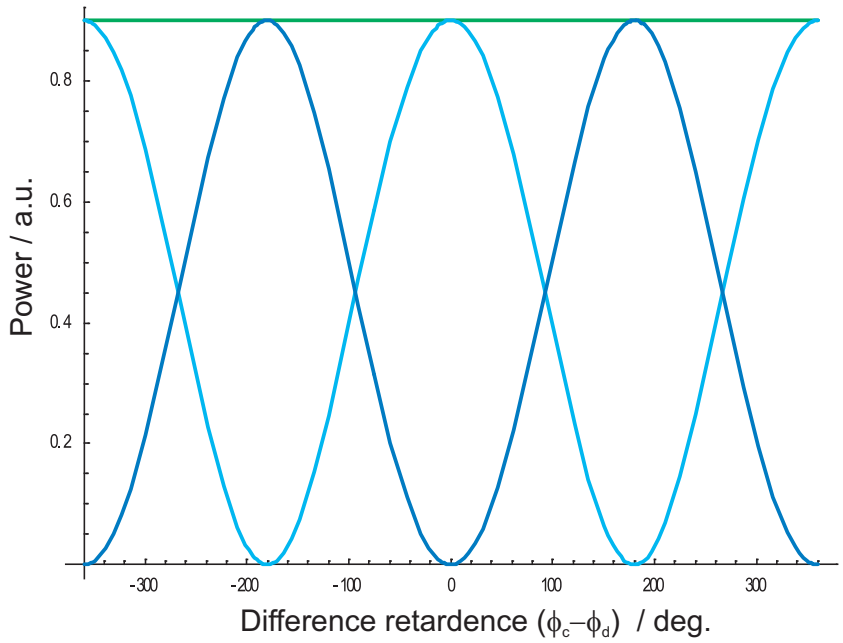

Figure 4.5: Simulation of the difference retardance scan versus intensity of the outgoing beam for a grating with the g parameter equal to 0.9 with the grating filter applied. The three curves represent scans done with the P and S orientated polarizer and without. The amplitudes of the scans for an S and P orientated polarizer are the same and the simulated scan without a polarizer is a constant flat function.

$$F_E(\phi) = \frac{g}{\sqrt{(\cos^2[\frac{\phi}{2}] + g^2 \sin^2[\frac{\phi}{2}])}} \tag{4.13}$$

The corrected intensities then will take the form of equations

$$\begin{aligned} I_{grat} &= I_0(\cos^2[\frac{\phi}{2}] + g^2 \sin^2[\frac{\phi}{2}]) \cdot \frac{g^2}{(\cos^2[\frac{\phi}{2}] + g^2 \sin^2[\frac{\phi}{2}])} = g^2 \\ I_{grat,Ppol} &= I_0 \frac{g^2 \cos^2[\frac{\phi}{2}]}{(\cos^2[\frac{\phi}{2}] + g^2 \sin^2[\frac{\phi}{2}])} \\ I_{grat,Spol} &= I_0 \frac{g^4 \sin^2[\frac{\phi}{2}]}{(\cos^2[\frac{\phi}{2}] + g^2 \sin^2[\frac{\phi}{2}])} \end{aligned} \tag{4.14}$$

The simulated intensities plotted in Figure 4.5 show, that without polarizer, no polarization dependent modulation will occur. The experimentally

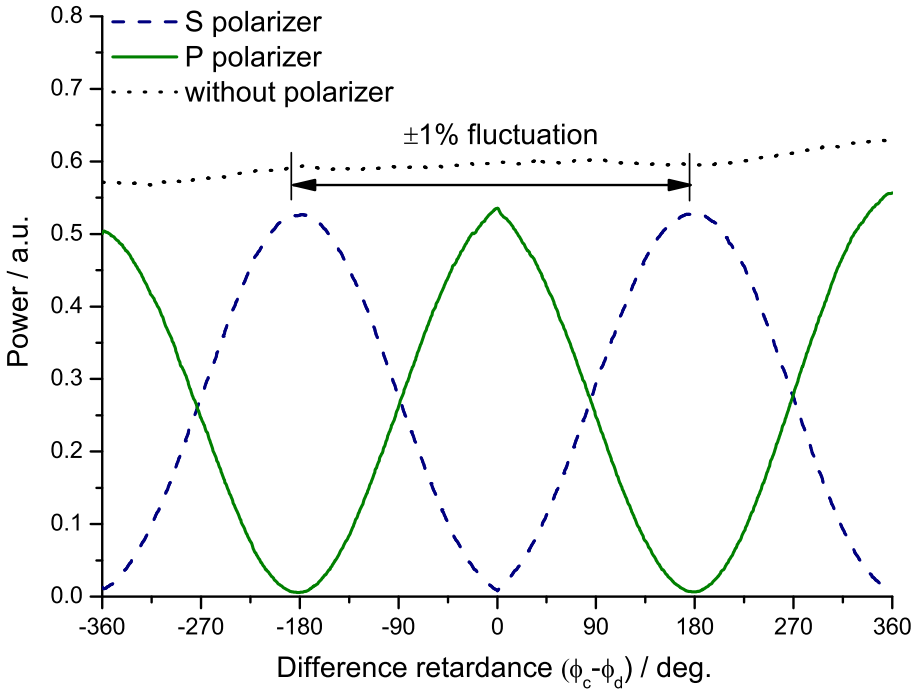

Figure 4.6: Scan of the difference retardance of a LC array versus transmission through the serial shaper and a polarizer with the amplitude filter applied. The scan done without polarizer shows no polarization dependent transmission of the setup.

performed scan 4.6 shows that the accuracy of the correction for the beam without polarizer results in a constant signal where the fluctuations within the range $(-180°, 180°)$ are on the order of 1%, which is comparable to the measurement noise.

The modulation of the S and P components are as well corrected and they are equal, but with the correction they cannot be described by sine or cosine functions of the retardances. It can be noticed that due to the applied filter function, the full width half maximum of the peaks for P components are different than for S. It may appear that enforcing the polarization dependent amplitude filter has changed the polarization state. At this point one has to remember that the cause of the change was the different reflectivity of

the of polarization components by the grating. Here, the amplitude filter influences both components simultaneously and equally, so the polarization state remains the same as described in 4.11 without grating correction.

To anticipate the elliptical polarization let us consider the ratio of the principal axes of a polarization ellipse. As mentioned before, for the serial shaper the accessible polarizations are limited to the ellipses with the principal axes orientated along the x and y coordinates. Therefore, the ratio is found by the absolute ratio of the Jones vector components. Without the influence of the grating this would be described by the function $\tan[\frac{\phi}{2}]$. For the grating with the relative efficiency parameter g, the ratio of the axes is given by

$$r = |g \tan[\frac{\phi}{2}]| \,. \tag{4.15}$$

It is easy to show that for nonzero g the ratio can change in the range $\{0, +\infty\}$, so it is always possible to manipulate the ellipticity regardless the polarization sensitive grating efficiency.

4.4 Pulses

Given the control over the polarization ratio, a few test pulses were generated and resolved. Since the polarization in this setup is restricted to states with the principal axes along the P or S directions, all pulse features can be obtained by recording them in these two directions. The time structure of the pulse is then acquired by measuring the crosscorrelation of the P and S polarization component with the unmodified reference linearly polarized pulse.

The first figure represents an unchanged pulse with the ratio parameter chosen to be $r = 0$, corresponding to linear P polarization. As required, the crosscorrelation of the P component is an intense single pulse and there is almost no signal in the S component.

The second figure displays a pulse with the same ratio, $r = 0$, but with an S linear polarization. Contrary to the previous example, the P crosscorrelation is flat, whereas the S is an intensive peak.

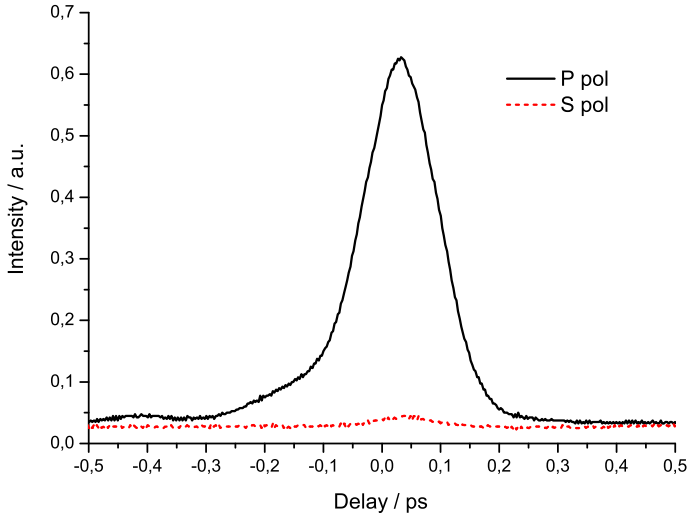

Figure 4.7: Crosscorrelation traces of a fs pulse polarized linearly and parallel to the plane of the optical table. The P component is dominant whereas there is almost no intensity in the S component.

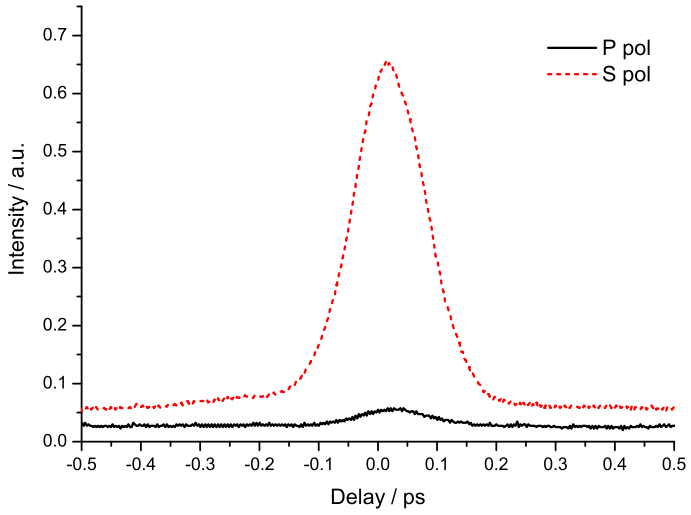

Figure 4.8: Crosscorrelation traces of a fs pulse polarized linearly and perpendicular to the plane of the optical table. The S component is dominant and there is very little intensity recorded for the P component.

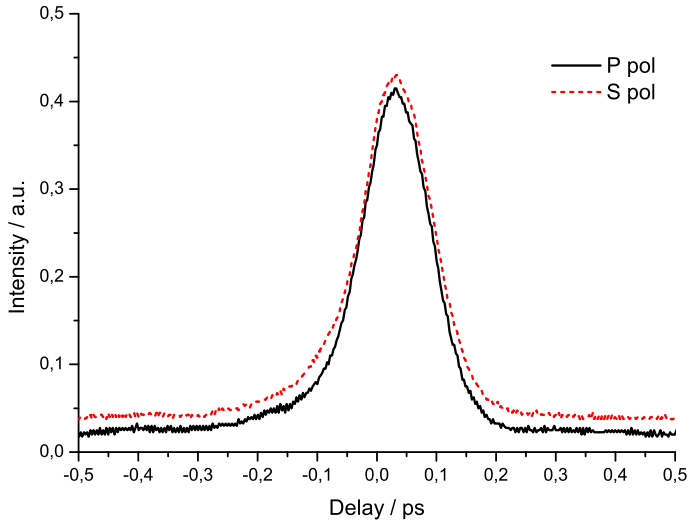

Figure 4.9: Crosscorrelation traces of a circularly polarized fs pulse. The polarization components are almost equal.

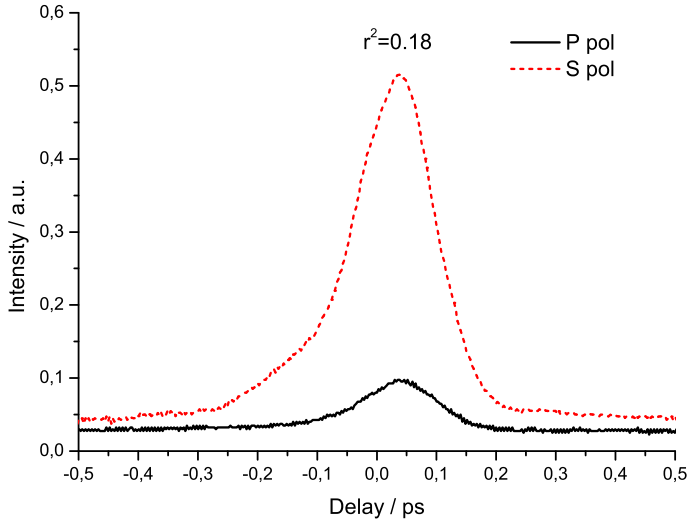

Figure 4.10: Crosscorrelation traces of a elliptically polarized fs pulse with $r = 0.41$.

Afterwards, the ratio was chosen to be equal one, implying circular polarization of the pulse. The crosscorrelation should be the same regardless the chosen polarization direction, which is the case.

The last crosscorrelation is an elliptically polarized pulse. The desired ratio was chosen to be 0.41 and the value from the crosscorrelation is 0.42, which is a very good agreement.

4.5 Test optimizations

After the basic tests of polarization manipulation, first genetic optimizations were performed in order to test the algorithm in the new search space which includes the polarization manipulation.

The transmission through the S orientated polarizer was the subject of the first optimization. The goal of this exercise was to see if the unmodified algorithm, which will be described later in Chapter 6 utilizes the new introduced possibilities. In other words, all the pixels are treated in the same way, regardless to which pass they belong. Without any modulator interaction the outgoing polarization is parallel and for this reason if a rise of the transmission through the S orientated polarizer is observed, the polarization was altered. As a feedback signal the intensity after the polarizer was recorded by a power meter. In this experiment the phase of the pulse does not play any role, so it is a matter of amplitude optimization in the first pass and polarization in the second. The rise in the transmitted light intensity through the generations is shown in Figure 4.11.

In the first stage of the process there is a fast rise in the signal, then it converges slowly to the optimum. The algorithm has succeeded, although it was still optimizing as it would manipulate the phase and the amplitude for a standard double layer shaper. The final pixel pattern displays regions of the first and the second pass on the modulator. The first pass is marked by a region of pixels where the amplitude is close to 1. When it comes to examining the second pass, Expression 4.9 defines, that the S polarization component is proportional to $\sin[\frac{(\phi_c-\phi_d)}{2}]$. Rendering the difference of the phase shifts should exhibit the same effect, as for the amplitude in the first pass. Indeed, when the S polarization component is yielded from the final

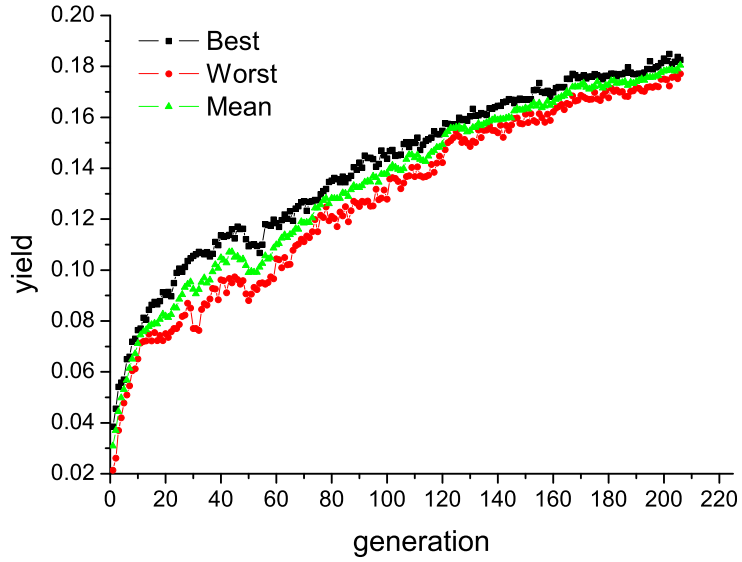

Figure 4.11: Optimization of intensity transmitted through an S orientated polarizer. The curves show the best, the mean, and the worst obtained transmitted intensity for every generation of a genetic algorithm.

retardances, the distinct pixels where the modulator is used in the second pass shows a polarization change from P to S. These results are presented in Figure 4.12.

The clear distinction between illuminated pixels and unused ones is much better visible in the "polarization" part of the array. The reason for incomplete convergence of the amplitude to one is most probably due to not enough generations performed. Disregarding the fact, that amplitude was not completely set to the maximum, it is not hard to see the exploited part of the modulator. Outside the actually used pixels the chosen values are random. Inside the illuminated "window" for the region of the first pass there is a flat structure of amplitudes close to one. In the second pass the same effect is observed for the S polarization. This simple test proves that polarization manipulation occurs and as well that the unmodified, so to say "unaware of the polarization" algorithm is able to adapt to the new gain capabilities.

In the next step the algorithm has been modified in a way that the first

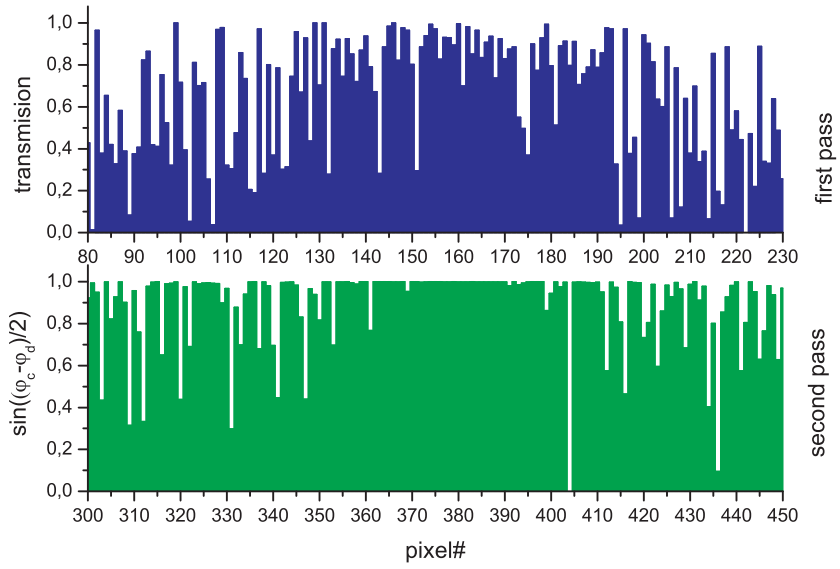

Figure 4.12: Amplitude mask for the first pass and extracted S polarization component for the second pass obtained during the optimization of the transmission through the S orientated polarizer. The regions shown on the graph are the ones containing the illuminated pixels (approx. 120 to 200 in the first pass and 340 to 420 in the second) close to illuminated pixels and their neighbors. The regular structure of pixels is the distinct of the exploited pixels from the rest.

and the second pass through the modulator are treated separately and that pixels used in these passes are paired for the matching wavelengths. Then, the first pass is programmed to handle the amplitude ($\cos[\frac{\phi_a-\phi_b}{2}]$) and the second pass to manage the the polarization state ($\begin{bmatrix} \cos[\frac{\phi_c-\phi_d}{2}] \\ i\sin[\frac{(\phi_c-\phi_d)}{2}] \end{bmatrix}$). The phase of the pulse is controlled by the sum of retardation of both passes ($\frac{1}{2}(\phi_a+\phi_b+\phi_c+\phi_d)$). From this point different types of optimizations can be performed within diverse search space, for example including only the phase or the amplitude or the polarization or any combination of these pulse features. The formalism of possible types of the optimization is presented in the table 4.1.

The modified algorithm with the options of restricting the optimized features of the pulse was tested on the second harmonic generation (SHG) [79] in a BBO crystal. This process takes advantage of the nonlinear properties

Table 4.1: Formalism of optimization types.

type	description	constrains
PAP	Phase, amplitude, and polarization	no restrictions
PAX	Phase and amplitude	$\phi_c - \phi_d = const.$
PXP	Phase and polarization	$\phi_a - \phi_b = const.$
XAP	Amplitude and polarization	$\phi_a + \phi_b + \phi_c + \phi_d = const.$
PXX	Phase	$\phi_a - \phi_b = const.$ and $\phi_c - \phi_d = const.$
XAX	Amplitude	$\phi_a + \phi_b + \phi_c + \phi_d = const.$ and $\phi_c - \phi_d = const.$
XXP	Polarization	$\phi_a + \phi_b + \phi_c + \phi_d = const.$ and $\phi_a - \phi_b = const.$

of some optical materials. The polarization of the medium induced by an electric field [80] has a nonlinear response which can be expanded in a power series of the electric field vector:

$$P = \chi^{(1)}E + \chi^{(2)}E^2 + \chi^{(3)}E^3 + c.c. \tag{4.16}$$

where $\chi^{(i)}$ are the following orders of nonlinear susceptibilities. Substituting in 4.16 $E = E_0 \sin(\omega t)$ and using the relation $\sin^2(\omega t) = \frac{1}{2}(1 - \cos(2\omega t))$ shows that for non-zero $\chi^{(2)}$ there is possible generation of the second harmonic of the fundamental frequency. The nonlinearity of the polarization response is not the only condition here [81]. The intensity of the second harmonic is given by the proportion:

$$I_{2\omega} \propto I_\omega^2 \omega^2 d^2 L^2 \frac{\sin^2[\frac{\Delta kL}{2}]}{[\frac{\Delta kL}{2}]^2} \tag{4.17}$$

where L is the medium length, $\Delta k = k_{2\omega} - 2k_\omega$ is the wave vector mismatch, and the parameter d denotes the nonlinear coefficient proportional to $|\chi^{(2)}|^2$. It is important to emphasize two dependencies from 4.17.

First, the intensity of the second harmonic (SH) is proportional to the square of the intensity of the fundamental wave. In the domain of fs pulses it means, that for pulses having the same energy, the shorter the pulse is, the higher the intensity becomes and consequently it leads to the increased efficiency of the process.

The second important relation comes from the fact that the maximum of the function

$$\sin^2[\frac{\Delta kL}{2}]/[\frac{\Delta kL}{2}]^2$$

is found for $\Delta k = 0$. This is called the phase matching condition and the use of $k = n_\omega \omega/c$ leads to $n^{(2\omega)} = n^{(\omega)}$. This condition is never fulfilled for the linear dispersion regime, since $n^{(2\omega)} > n^{(\omega)}$. The consequence of phase mismatch is that at some point in space the phase difference between the fundamental wave and its second generation will reach 180°, and the process of coherent generation will stop and then reverse. Phase matching condition can be realized by exploiting birefringence [82] (double refraction) of some anisotropic materials, where an optical axis is pronounced. Light perpendicular polarized to the plane defined by the optical axis and the

wave vector will be affected by the ordinary refractive index n_o, but if it is polarized in that extraordinary plane, then it will be influenced by the extraordinary index of refraction n_e. Moreover, the extraordinary index is as well dependent from the angle ϑ between the wave vector and the optical axis.

$$\frac{1}{n_e^2(\vartheta)} = \frac{\cos^2(\vartheta)}{n_o^2} + \frac{\sin^2(\vartheta)}{n_e^2} \tag{4.18}$$

This yields the equation for the refractive index.

$$n_e(\vartheta) = \frac{n_e n_o}{\sqrt{n_o^2 \sin^2(\vartheta) + n_e^2 \cos^2(\vartheta)}} \tag{4.19}$$

As Equation 4.19 indicates, the extraordinary index of refraction can be tuned by varying the angle ϑ at the same time preserving a constant ordinary index. Keeping in mind the relation $n_{2\omega} > n_\omega$ for a medium with a negative birefringence ($n_e < n_o$) one can find ϑ_m for which

$$n_e^{(2\omega)}(\vartheta_m) = n_0^{(\omega)} \tag{4.20}$$

and thus the phase matching condition will be met. The index surfaces for the fundamental and the second harmonic wave are shown in Figure 4.13 to clarify the concept of phase matching and phase matching angle in a birefringent media.

The phase matching angle can be found geometrically by intersecting the index surface of the extraordinary second harmonic wave and the index surface of the ordinary fundamental wave. This is Type I of second harmonic [79] generation and it involves two photons at the fundamental frequency polarized in the ordinary plane in order to produce one SH photon of extraordinary polarization. Therefore phase matching requires an alignment of the polarization of the fundamental wave in the ordinary plane for an efficient generation. In case of different orientation of polarization only a projection of the electric field vector on the ordinary plane will be efficiently transformed to the second harmonic. Thus, the efficiency is proportional to $\cos(\gamma)$, where γ is the mismatch angle between polarization orientation and the crystal ordinary plane.

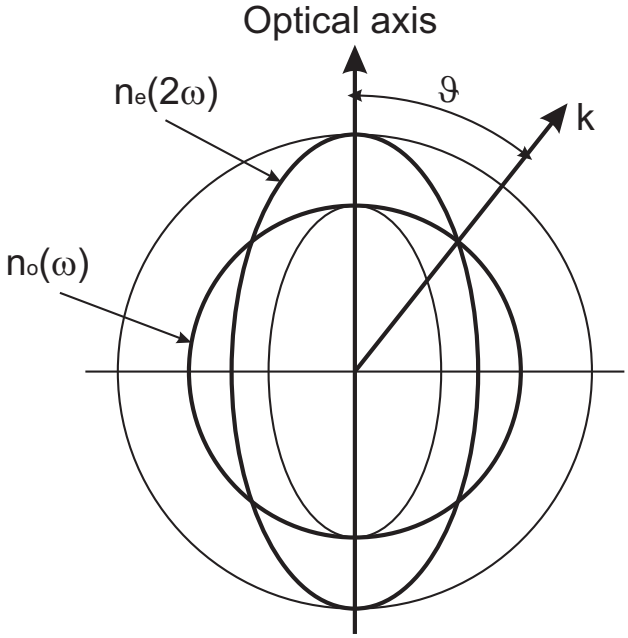

Figure 4.13: Index surfaces for ordinary and extraordinary rays drawn for frequencies ω and 2ω. The optimal phase matching angle is indicated between the vector k and the optical axis.

Summarizing, the SHG depends strongly on the intensity of the fundamental wave and the phase matching. The peak intensity is controlled in our experiment by the amplitude and phase, which determines the pulse duration. The phase matching is influenced by the polarization state of the fs-pulse.

The experiment was performed with the MIRA Seed oscillator from Coherent. Femtosecond pulses with the central wavelength aligned at 780 nm and a bandwidth of 30 nm were passing through the serial setup. Then the beam was focused by a lens of 150 mm focal length. Near the focus the BBO crystal was placed. For the alignment, the polarization was rotated by an waveplate by 90° from P and then the crystal orientation was adjusted for the most efficient SH generation. After the generation of SH the residual fundamental frequency needed to be separated from the SH in order to get a clear feedback signal from the photodiode placed afterwards in the beam. To do so, a highly reflective mirror designed for the fundamental wavelength was placed in the beam. With this method the extinction of the fundamental

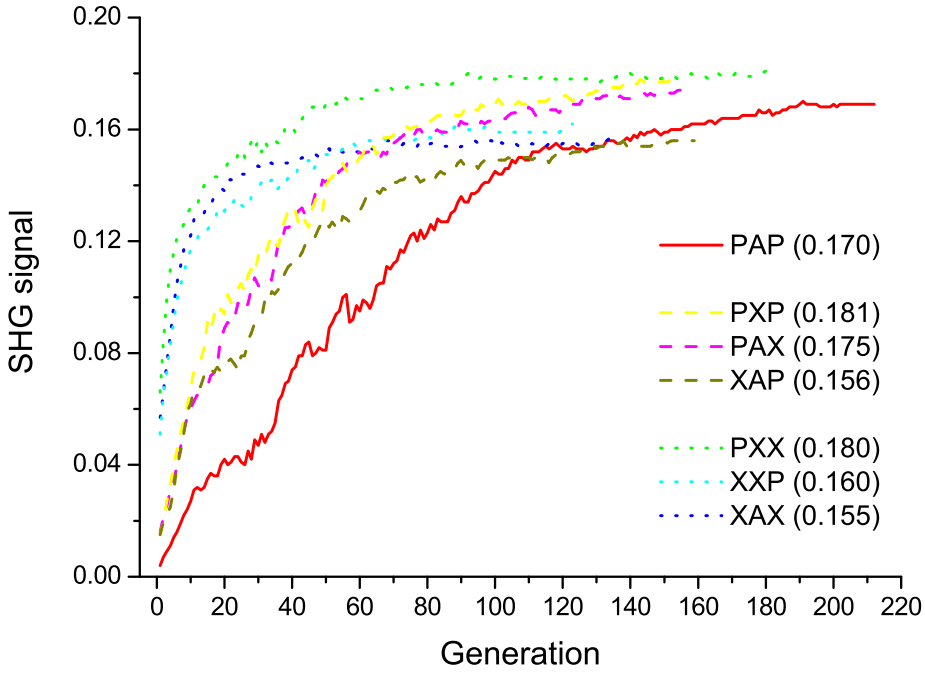

Figure 4.14: Comparison of different types of second harmonic optimization in a nonlinear crystal. The presented curves show optimization courses for optimizations with different parameters optimized, one of three (PXX, XAX, XXP), two (PAX, PXP, XAP), or all (PAP). The values in the inset describe the signal obtained at the end of the given optimization.

wave is much higher than by applying a BG39 filter. After setting crystal and diode, the wave plate was removed from the beam, so the initial polarization was P. In other words, the starting condition had been chosen in a way that the algorithm had to change polarization, in addition to maximizing the intensity of the optimized pulse. Naturally, an exception was made for the optimizations without the possibility of polarization manipulation, where the waveplate was again placed in the beam before the crystal.

Different types of optimizations introduced in table 4.1 had been performed in order to increase the second harmonic generation. The course of these optimizations is presented in Figure 4.14. There are two characteris-

tics of the optimization course, that allow to divide the optimizations into 3 categories. The distinction can be made based on the signal rise or the convergence speed and the starting value. The fast convergence and a higher starting yield of SHG is observed when only one feature (PXX, XAX, XXP) of the pulse is being optimized. A moderate rise is recorded in optimizations with two parameters (XAP, PXP, PAX), and a slow rise for the PAP optimization. Such a clear relation of the convergence speed with the number of parameters to optimize is expected. It is obvious that finding the best possible solution will be faster in case of a smaller search space, which is the case with the PXX, XAX, and XXP optimizations. The higher starting values of those optimizations can be explained by the same mechanism. For the fixed parameter of a given optimization it is chosen at optimal condition, for example the PXP optimization is done for transmission set to 1. Another way to see this is to assume that all of these search spaces include the same optimal solution and therefore a random pulse from a larger space is more likely to yield a worse SH signal. This assumption may not be entirely correct when the outgoing fs pulses from the passive shaper are not transform limited. There could be two reasons for this, the chirp of the incoming pulse and imperfect alignment of the shaper. Then the end result for the optimizations including phase manipulation which will correct the phase of the pulses and thus will gain more signal in the end than the rest. As one can see the end values differ slightly. The higher factors belong to optimizations with the possibility of phase manipulation. It means that there is a common global optimum which can be reached for those optimizations with optional change of the phase, and a local one for all the rest. A difference of the end value is clearly visible by comparing the PXX with the XAX and XXP curves. This suggests, that end values should then be divided in two distinct groups. Probably this would be the case if the PAP optimization would be left to fully converge. Yet this effect of the distorted phase of the pulse does not affect the different search space size consequences which are pronounced in the convergence speed and the start values.

4.6 Summary

The Chapter described a scheme of independent control over the phase, the amplitude, and the polarization of fs pulses, including theoretical analysis and experimental realization. First, the Jones calculus was employed to demonstrate light interaction with liquid crystals with crossed axes like in commercial double layer modulators. The possibilities as well as limitations of such a confinement were shown. When using the crystals with the optical axis aligned at 45° or −45° shaping is limited to elliptical polarizations with the major axis orientated parallel or perpendicular to the incoming light polarization. Moreover, a double layer modulator is capable either of phase and polarization modulation or phase and amplitude modulation when it includes a polarizer. Therefore, to achieve simultaneous control over phase, amplitude, and polarization a minimum of three arrays and a polarizer are necessary. Such an arrangement as well as the combination of two double layer modulators with a polarizer in between them are studied. Next, the experimental setup based on the combination of a phase and amplitude shaper with a phase and polarization setup is demonstrated. Instead of using two shapers combined one after the other, one modulator with broad arrays is used in a two pass configuration. In this setup, the efficiency of the last reflection on the grating is polarization sensitive, therefore a software solution is implemented to counteract this effect. After achieving independent polarization and amplitude modulation, simple polarization shaped pulses are generated and resolved with a good agreement with the target pulses. As a last part of this Chapter, a few optimizations are performed as a test of an used algorithm. The transmission through a polarizer crossed with the initial outgoing polarization is optimized, which demands for an optimal amplitude and polarization, and is independent from the phase. Then, the second harmonic generation is optimized as a test of all accessible degrees of freedom of the pulse shape. Both optimization types show convergence to the obvious optimal solutions.

To conclude, the serial setup is robust and relatively easy to align in comparison to the parallel shaper presented in Chapter 3, but it is not capable of a changing the spectral polarization orientation and therefore can not be

applied to more general applications.